A Thesis Presented to

The Faculty of Alfred University

The Effect of Bioactive Glass Particle Size on Sintering

Audrey Hepp

In Partial Fulfillment of

the Requirements for

The Alfred University Honors Program

Date May 10, 2013

Under the Supervision of:

Chair: Dr. Matthew Hall

Committee Members:

Dr. Anthony Wren

Dr. Aisling Coughlan

Acknowledgements

I would like to express my sincere appreciation to my advisor and committee chair Dr. Matthew Hall, for his support and guidance throughout my research here at Alfred University. His knowledge, enthusiasm, and counseling are second to none.

I would also like to acknowledge with much gratitude my committee members Dr. Anthony Wren and Dr. Aisling Coughlan for their time and patience with my never-ending questions.

Last but not least, I would like to thank Swavek Zdzieszynski for his help preparing my samples for XRD analysis.

Table of Contents

List of Tables

List of Figures

Abstract

45S5 is a bioactive glass that has recently shown promise as a bone tissue scaffold material. In order to be used in this manner, the glass must be sintered. Studies have shown that the sintering behavior of a number of materials is affected by particle size. However, the effect of bioactive glass particle size on sintering behavior had, to this point, not been studied at in any depth. The purpose of this research, then, was to determine the effects of particle size on the sintering of 45S5. Results suggest that particle size does affect the sintering behavior of 45S5, and that there is likely an interaction effect between particle size and crystallinity that led to the 53-63μm 45S5 having the lowest sintering temperature.

I. Introduction

A bioactive material is one that is designed to have high biocompatibility[1] and to induce specific biological responses[2]. Bioctive glasses are glasses that, when used in biomedical applications, are "active in the body and stimulate the natural healing of damaged tissues"[3]. When implanted into the body, a calcium phosphate-rich surface layer[1] similar to hydroxyapatite (the mineral constituent of bone) forms and facilitates the bonding of the implant with hard or soft tissue[2]. As the dissolution of the material progresses, it provides not only space for tissue in-growth, but also stimulates the production of new tissue via the precipitation of ions[1,3,4].

The first glass composition found to form a direct bond with bone was given the name Bioglass®[1-6]. It was discovered by Dr. Larry Hench in 1969 at the University of Florida in Gainesville under funding from the US Army Medical Research and Development Command[5]. Dr. Hench chose a soda-lime-phosphosilicate[3] glass composition of 45 SiO_2 – 24.5 Na_2O – 24.5 CaO – 6 P_2O_5 (wt%). Small rectangular sections of the glass were implanted in rat femurs, and at the end of six weeks, the following was reported:

> "These ceramic implants will not come out of the bone. They are bonded in place. I can shove them, I can hit them and they do not move. The controls easily slide out."[5]

Further testing revealed that Dr. Hench's glass released dissolution products that stimulated the differentiation of osteoblasts by stimulating specific genes[3]. Thus, bioglass is both osteoconductive and osteoinductive[6].

45S5 bioglass is the specific formulation (45 SiO_2 – 24.5 Na_2O – 24.5 CaO – 6 P_2O_5 (wt%)) created by Dr. Hench. However, there are a number of other bioglass formulations available, such as NovaBone® and Perioglas®[5]. These bioglasses are most widely used in periodontal and orthopedic applications[3] as a bone filling material[7]. They stimulate healing and induce regeneration of bone tissue[3]. NovaMin®, a fine particulate

form of bioglass, is the active ingredient in Sensodyne Repair and Protect, a toothpaste designed to reduce tooth sensitivity. The bioglass particulates release ions that induce the precipitation of a mineral layer similar to hydroxapatite, and similar to tooth enamel, on top of the inner dentine tubules that lead to the nerve endings in teeth. This mineral layer blocks the tubules, preventing the pain that is felt when hot or cold liquid flows down the tubules to the nerves[3,8].

Recent research into 45S5 has shown its great potential as a bone tissue scaffold material[2-6]. These tissue scaffolds are engineered such that their functionality mimics that of the extracellular matrix (ECM) of bone. The ECM plays a crucial role in bone morphogenesis by providing an appropriate microenvironment for the growth of new bone. The tissue scaffold essentially acts as a temporary ECM[9]. As the tissue scaffold gradually dissolves, its dissolution products are resorbed, and the scaffold itself is replaced by new bone[4,9].

Qizhi et al. report three characteristics of 45S5 that make it a very suitable material for the construction of bone tissue scaffolds: the rate of biodegradation is able to be controlled, it is osteoconductive and bioactive, and it has an ability to deliver cells[10]. 45S5 has also shown promise as a bone tissue scaffold material because it is osteoinductive[6] and can be formed into a highly porous structure[9,10]. Therefore, the 45S5 scaffold not only integrates with host bone while allowing bone ingrowth, but also helps assist in the healing of bone[9] by promoting the differentiation of osteoblasts[3]. Additionally, 45S5 bioglass exhibits antibacterial effects against a number of bacteria (including *S. aureus, S. epidermidis, and E. coli*) due the high aqueous pH that results as dissolution progresses[7].

To make these bone tissue scaffolds, the 45S5 glass must be in powder (frit) form[9]. The glass particles are formed into the desired 3-D geometry, typically by foam replication, and sintered[11]. Sintering of 45S5 facilitates strong particle bonding into a glass phase[2,3].

Sintering is a necessary and crucial step in the process of creating bone tissue scaffolds[3]. Keeping that in mind, it has been shown that particle size does have an effect on sintering[3,12,13]. Smaller particle sizes tend to sinter more easily (at a quicker rate) because of their increased surface area[3,13]. It has been shown for Ti-6Al-4V powders that as particle size increases, sintering temperature also increases[13].

Francis et al. undertook a study to examine the effects of particle size on flash sintering of yttria stabilized zirconia. It was discovered that larger particle sizes induced a higher resistance to sintering, that is, a higher furnace temperature was required. Further, this study showed that sintered density decreases as particle size increases[14]. Similar results are found in a number of other materials[3,13,12]. Density is another important attribute in bone tissue scaffolds, as the ideal scaffold will have a density and compressive strength similar to that of bone[10].

It is clear, then, that particle size has a direct effect on the sintering behavior of a number of materials. Sintering behavior itself has a clear role in the construction of 45S5 bioglass bone tissue scaffolds. The direct impact of particle size on 45S5 sintering, however, has not yet been researched in any depth. Thus, the objective of this work is to investigate the influence of particle size on the sintering behavior of 45S5 bioglass.

II. Experimental Procedure

A. Creation of 45S5 Frit

45S5 bioglass requires the following raw materials: $NaCO_3$, $CaCO_3$, $NH_4H_2PO_4$, and SiO_2. Table 1 lists the amount (in grams) of each raw material required to create a batch that would yield 150g of 45S5 bioglass. Each of these raw materials was measured on an Ohaus Voyager scale and deposited into a high density polyethylene (HDPE) container. After all raw materials were combined in the container, milling media was added, and the container was vigorously shaken to ensure the thorough mixture of all materials. The milling media was then removed, and the raw 45S5 was ready for melting.

Table 1. Raw materials required to form 45S5 bioglass.

45S5 Oxide	Wt%	Raw Material	Amount Needed to Yield 150g 45S5 Glass
Na_2O	24.5	Na_2CO_3	62.845
CaO	24.5	$CaCO_3$	65.591
P_2O_5	6	$NH_4H_2PO_4$	14.586
SiO_2	45	SiO_2	67.500

A Thermo Scientific Lindberg Blue M furnace and a platinum crucible were used to melt the 45S5. Due to the large quantity of 45S5 and the smaller size of the platinum crucible, the raw 45S5 needed to be broken up into three batches and melted separately. For each batch, the raw 45S5 was poured into the crucible and added to the 1400°C furnace for one hour. At the end of that hour, the crucible was removed from the furnace, and the melted glass was poured into a bucket of water to quench it.

The newly quenched 45S5 bioglass was then removed from the water and stored in an HDPE container in a desiccator to prevent any absorption of water.

The full 150g of 45S5 was placed in a Gy-Ro mill. The mill was run in short bursts (8.5 seconds) until the 45S5 glass was fully powdered. This resultant powder is referred to as frit. The frit needed to be separated based on particle size. The following sieve sizes (diameter) were used: 32 µm, 38 µm, 45 µm, 53 µm, 63 µm, 75 µm, 90 µm, and 106 µm. Table 2 lists these sieve sizes and their ASTM equivalences. These sieves were arranged in a Gilson Performer III SS-3 automatic shaker. The 45S5 frit was added to the top sieve, and the column of sieves was vibrated on high for one hour.

This provided particle size diameter ranges of 32-38 µm, 38-45 µm, 45-53 µm, 53-63 µm, 63-75 µm, 75-90 µm, and 90-106 µm. Again, due to the hygroscopic nature of 45S5, all samples were stored in a desiccator when not in use.

Table 2. ASTM and US Standard sieve sizes used to differentiate 45S5 particle size.

ASTM No.	US Standard
450	32 µm
400	38 µm
325	45 µm
270	53 µm
230	63 µm
200	75 µm
170	90 µm
140	106 µm

B. HSM and XRD Measurements

A Misura HSM-ODHT, a heating microscope with attached vertical optical dilatometer, was used for all hot-stage microscopy measurements. The HSM sample is made up of a 45S5 powder samples that were hand pressed into cylinders 3 mm in height and 2 mm in diameter. Each cylinder was placed on an alumina substrate to be loaded into the HSM.

A cylindrical sample from each particle size range was heated up to 1,300°C at a rate of 10°C/minute. Images were taken for each increase in 1°C from 400°C up to 1300°C. The Misura HSM analysis software was used to determine softening, sintering, and melting temperatures. Additionally, sphere and half-sphere temperatures were determined when possible. A new cylindrical sample from each particle size range was heated up to 1300°C but at a rate of 5°C/minute. Images and analysis were obtained in the same manner as the previous samples.

Upon samples' heating to 1,300°C in the Misura HSM, each alumina substrate with melted 45S5 glass on it was retained and stored. Three of these fully melted glass samples (32-38 μm, 53-63 μm, and 90-106 μm) were then analyzed using X-ray diffraction.

Mounting putty was used to mount samples onto a plastic sample holder. X-ray diffraction was measured via Cu radiation using a Bruker D2 Phaser with the following scanning parameters: 5°-75° 2θ range, step size of 0.04041520, 2 seconds dwell time, goniometer distance of 282 mm, voltage of 30 kV, 10 mA current, 30 rpm.

The resulting patterns were then analyzed using X'Pert Highscore Plus, a pattern analysis software, with the following peak search parameters: minimum significance 2.00, minimum tip width 0.01° 2θ, maximum tip width 1.00° 2θ, peak base width 2.00° 2θ, and minimum 2nd derivative. The background was determined and

subtracted using a bending factor of 5, granularity of 20. Peaks were searched for and matched according to the Powder Diffraction File (PDF) database as provided by the International Center for Diffraction Data (ICDD) patterns Alumina peaks were identified first, followed by the 45S5 peaks.

III. Results

A. HSM

HSM analysis provided softening, sintering, and melting temperatures for all samples heated to 1300°C at a rate of 10°C/min. As particle size increased, the sintering temperature went from 1040°C, to 1032°C, to 1026°C, to 1016°C, to 1040°C, to 1058°C, to 1060°C. The softening temperature went from

The melting temperature remained relatively constant, ranging from 1202°C to 1208°C. This data is provided in Table 3.

Table 3. HSM data for 45S5 samples heated to 1300°C at a rate of 10°C/min.

Particle Size Range	Sintering Temperature (°C)	Softening Temperature (°C)	Melting Temperature (°C)
32-38 μm	1040	1152	1203
38-45 μm	1032	1191	1202
45-53 μm	1026	1108	1208
53-63 μm	1016	1066	1206
63-75 μm	1040	1103	1205
75-90 μm	1058	1180	1201
90-106 μm	1060	1203	1204

Changes in the height of the sample during heating, as measured by the dilatometer, were similar for all particle size ranges (Figure 1). All HSM images for samples heated at a rate of 10°C/min are listed in Appendix 1.

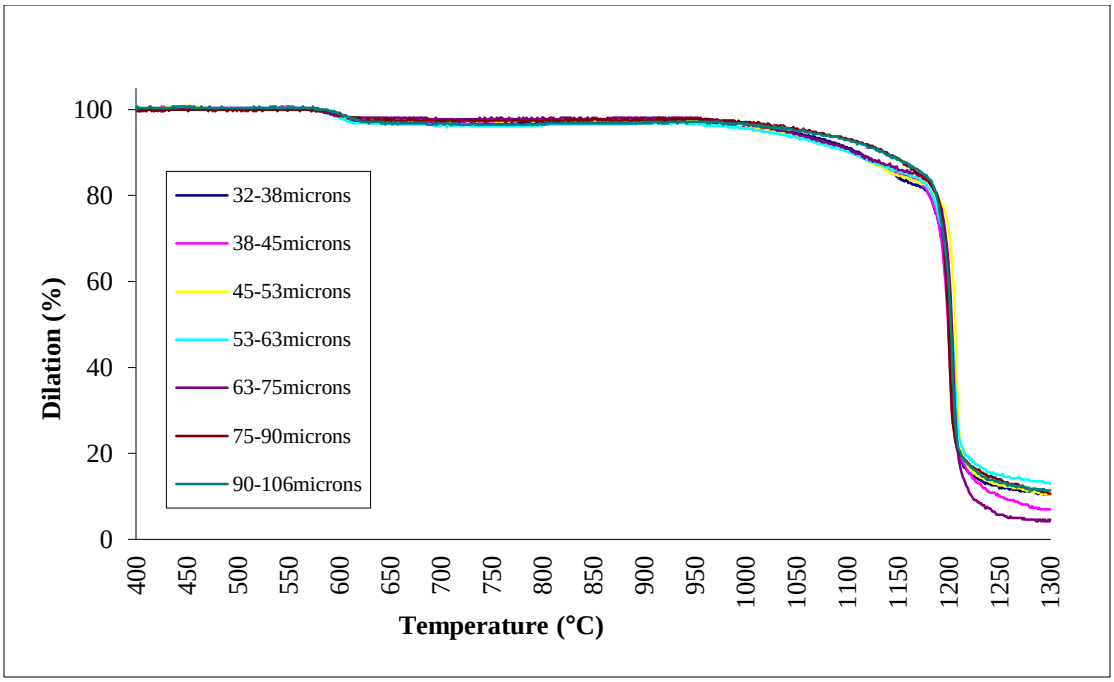

Figure 1. Height of 45S5 samples upon heating at a rate of 10°C/min in an HSM.

Table 4 shows the sintering, softening, and melting temperatures of all samples upon heating at a rate of 5°C/min. As particle size increased, the sintering temperature went from 1033°C, to 1019°C, to 1012°C, to 974°C, to 1017°C, to 1088°C, to 1060°C. The softening temperatures ranged from 1013°C, to 1201°C while the melting temperatures remained ranged from 1189°C to 1205°C.

Table 4. HSM data for 45S5 samples heated to 1300°C at a rate of 5°C/min.

Particle Size Range	Sintering Temperature (°C)	Softening Temperature (°C)	Melting Temperature (°C)
32-38 µm	1033	1165	1197
38-45 µm	1019	1201	1202
45-53 µm	1012	1187	1199
53-63 µm	974	1013	1189
63-75 µm	1017	1125	1205
75-90 µm	1088	1190	1201
90-106 µm	1060	1111	1199

Changes in the height of the sample during heating, as measured by the dilatometer, were similar for all particle size ranges (Figure 2). All HSM images for samples heated at a rate of 5°C/min are listed in Appendix 1.

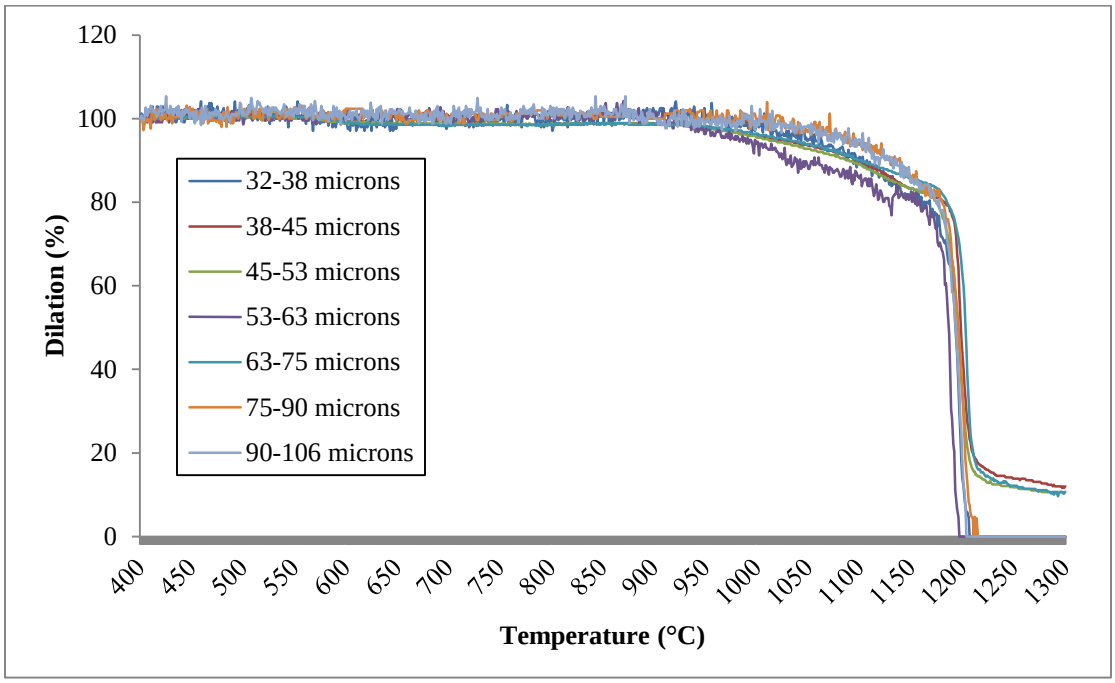

Figure 2. Height of 45S5 samples upon heating at a rate of 5°C/min in an HSM.

A graph of the sintering temperature vs. particle size is provided in Figure 3. This contains the sintering temperatures for all samples heated at 10°C/min and at 5°C/min as determined by the HSM.

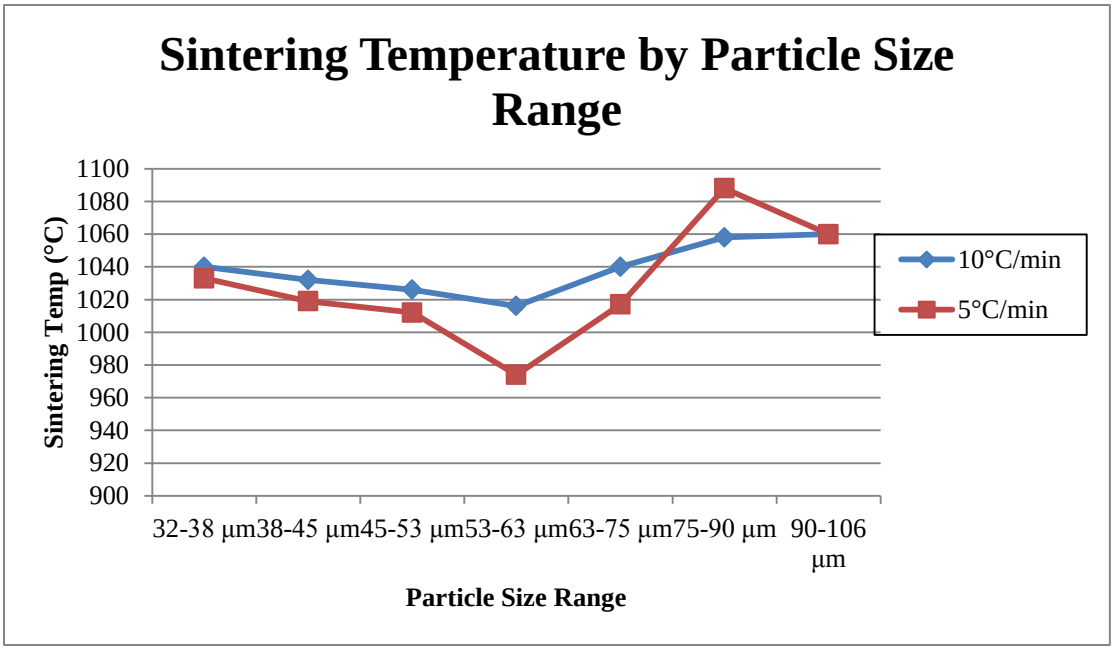

Figure 3. Sintering temperature for each sample based on particle size range and heating rate.

B. XRD

The X-ray diffraction pattern obtained for the 32-38 µm sample following heating to 1300°C at 10°C/min is shown in Figure 4. Numerous alumina peaks, the material of which the substrate was made, are present. Two crystallized 45S5 peaks are labeled at 21°2θ and 41°2θ.

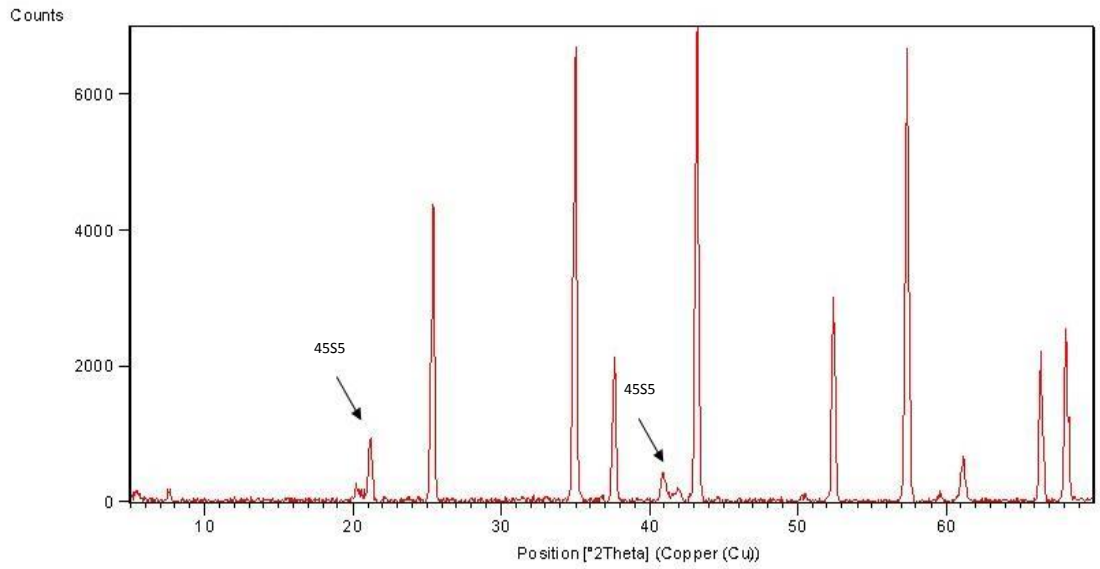

Figure 4. XRD pattern for 32-38 µm sample. 45S5 peaks are shown with an arrow, all others are alumina peaks.

Figures 5 and 6 show similar diffraction patterns for the 53-63 µm and the 90-106 µm samples following heating to 1300°C at 10°C/min. Again, two 45S5 peaks are labeled at 21°2θ and 41°2θ.

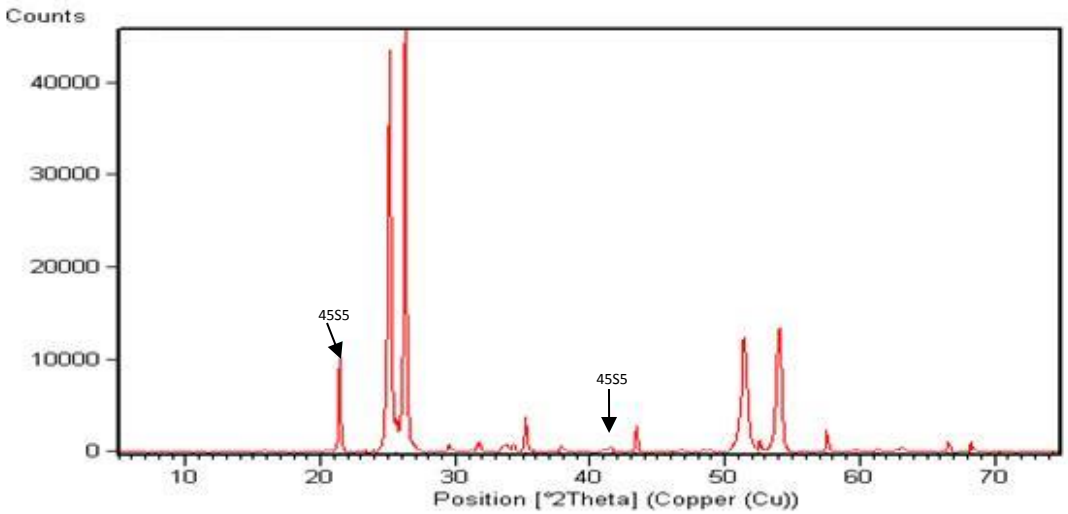

Figure 5. XRD pattern for 53-63 µm sample. 45S5 peaks are shown with an arrow, all others are alumina peaks.

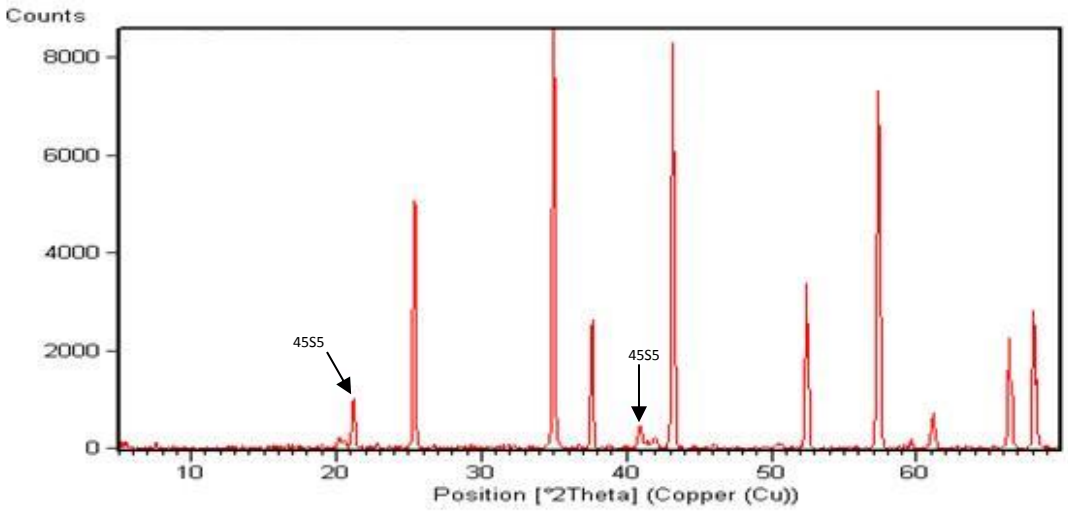

Figure 6. XRD pattern for 90-106 µm sample. 45S5 peaks are shown with an arrow, all others are alumina peaks.

IV. Discussion

The data collected shows that for particle sizes below the 53-63 μm range, sintering temperature tends to decreases as particle size increases. While for particle sizes above the 53-63 μm range, sintering temperature tends to increase as particle size increases. This suggests that (i) regardless of heating rate, particle sizes within 53-63 μm will have a lower sintering temperature than any other particle size between 32-106 μm, and (ii) it is likely that there is an interaction effect between particle size and the crystallization of the 45S5 while it is being heated.

It is clear from the crystalline 45S5 peaks in the X-ray diffraction patterns obtained that the 45S5 has crystallized to some extent in each sample. This further supports the supposition that there are interaction effects occurring between particle size and crystallization.

Because it is a glass, 45S5 crystallizes during heat treatment[3,4,10,11,15]. Crystallization of 45S5 is influenced by a number of parameters[16,17], including particle size[15] and viscous flow[10], which controls surface vs. bulk crystallization[15]. Bretcanu et al. showed that 45S5 is highly crystallizable and begins to crystallize around 650-700°C when it has a mean particle size <5μm. At this particle size, 45S5 crystallizes via surface crystallization[11]. However, with courser particles (300-500 μm), the crystallization mechanism of 45S5 shifts from primarily surface to primarily bulk crystallization[15]. Samples with particle sizes that lie somewhere in the middle of this range will likely have some mixture of surface and bulk crystallization.

Lefebvre et al. showed that at the onset of bulk crystallization in 45S5 between 600-700°C, there is “a complete inhibition of sintering” followed by a “minor shrinkage effect” until the glass transition temperature is reached and sintering resumes. Essentially, bulk crystallization inhibits sintering to some extent by inhibiting viscous flow[18].

This would seem to indicate that as particle size increases, sintering temperature will also increase, which fits in with the data from the 53-63 μm range and up. However, it contradicts with the data below the 53-63 μm range. This suggests that particle size and crystallization interaction effects, though they are not known at this time, play a large part in the sintering behavior of 45S5.

V. Conclusions

Upon heating in an HSM at a rate of 10°C/min, the sintering temperature of 45S5 bioglass decreased with increasing particle size from the 32-38 μm to the 53-63 μm range. Subsequently, the sintering temperature increased with increasing particle size from the 53-63 μm range to the 90-106 μm range. Results were similar upon heating at a rate of 5°C/min. X-ray diffraction patterns of samples following heat treatment indicated that crystallization had occurred.

This suggests that the reason the sintering temperature curves form a "u-shape" as particle size increases could be that there are interaction effects between particle size and crystallization during sintering. It is known that crystallization of 45S5 affects sintering[18]. It is also known that for a number of materials, particle size affects sintering[12]. However, the interaction effect of crystallization and particle size on the sintering of 45S5 bioglass is unclear.

The fabrication of effective 45S5 bone tissue scaffolds relies heavily on the controllability of the sintering behavior. Knowing that 45S5 particle size does influence the sintering temperature helps to increase the amount of control engineers have over the construction of 45S5 scaffolds.

VI. Suggestions for Future Work

Understanding how 45S5 particle size and crystallization interact during sintering is crucial when engineering bone tissue scaffolds. In order to fully understand this interaction, a number of future studies can be suggested.

Analysis via X-ray diffraction of 45S5 samples removed from a furnace at the onset of sintering could likely provide the percent crystallinity of the sample at the point of sintering. This might help to explain how the crystallization of the glass is affecting the sintering temperature of the sample.

Similarly, high temperature X-ray diffraction could yield useful results. High temperature X-ray diffractometers provide analysis of material behavior in-situ as a function of temperature[19]. This might allow for the determination of the exact temperature that crystallization begins and the temperature at which the sample fully crystallizes. Examining 45S5 samples of different particle sizes could potentially provide information on the interaction of 45S5 particle size and crystallization during sintering.

The optimal engineering of 45S5 bone tissue scaffolds could then be investigated using this information. It may be possible to create a 45S5 scaffold that has mechanical, structural, and biological properties that are nearly identical to the type of bone for which they will be used (trabecular vs. cortical bone) when particle size and crystallization effects on sintering behavior are considered.

VII. Appendix I

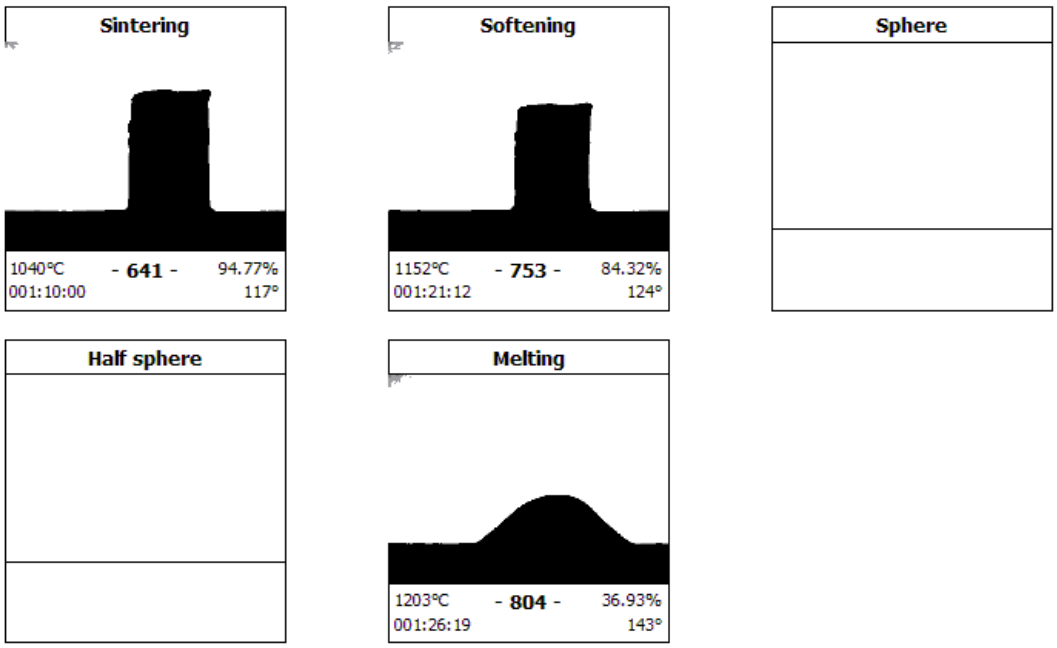

Figure 1. 32-38 µm heated at 10°C/min

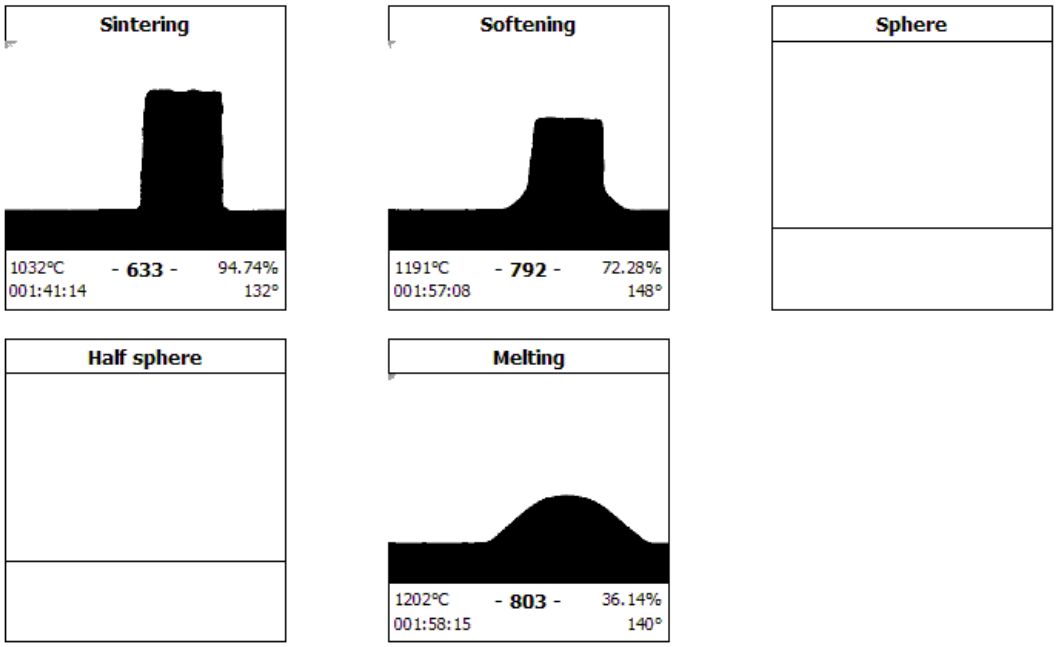

Figure 2. 38-45 µm heated at 10°C/min.

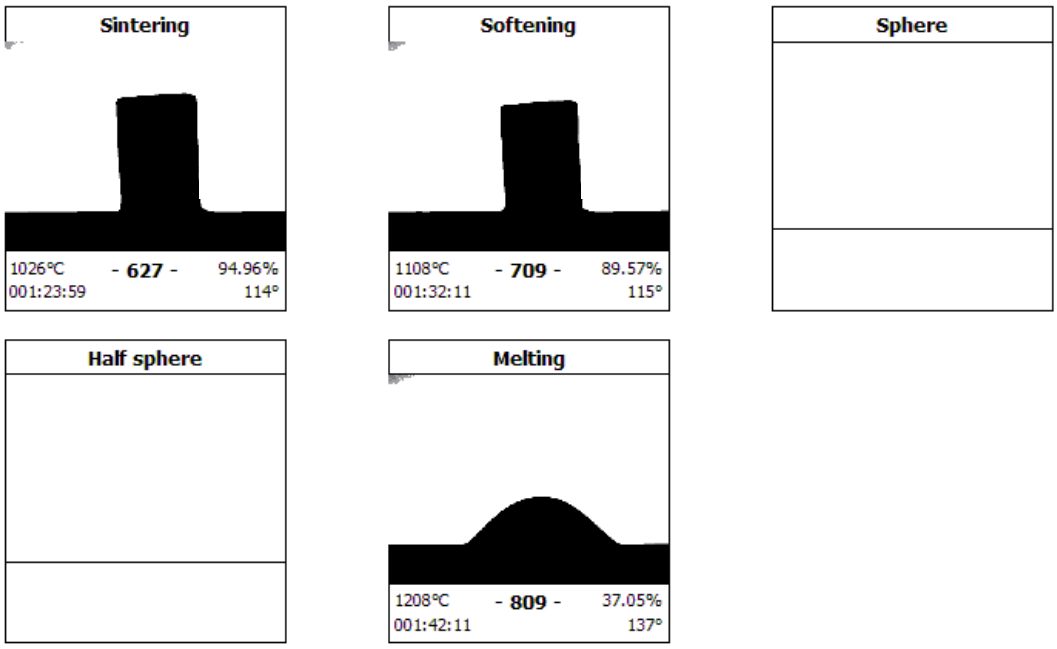

Figure 3. 45-53 µm heated at 10°C/min.

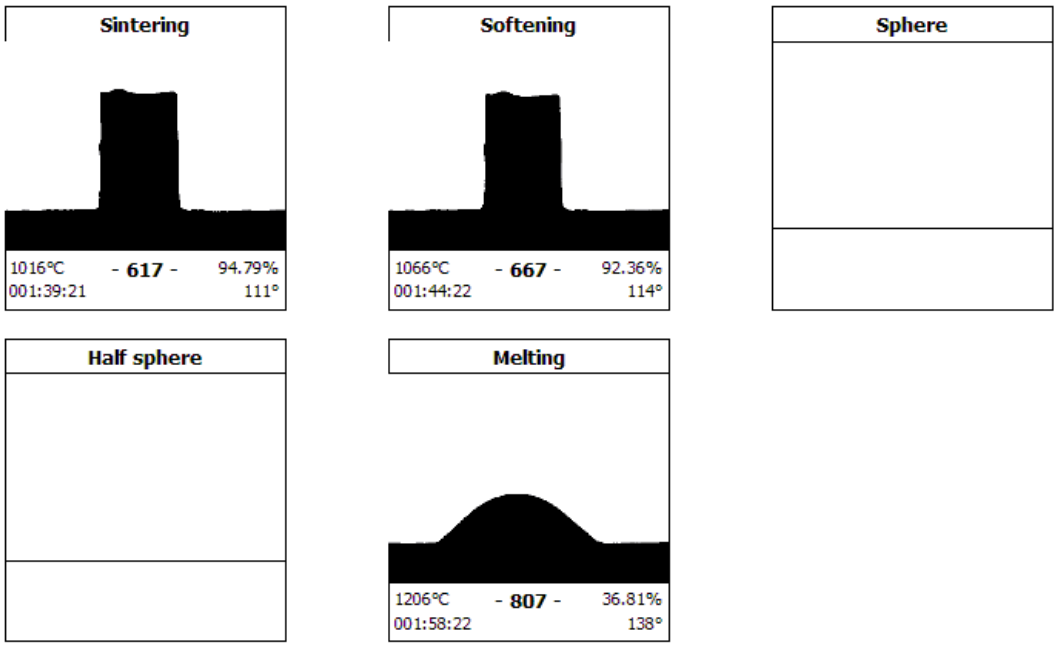

Figure 4. 53-63 µm heated at 10°C/min.

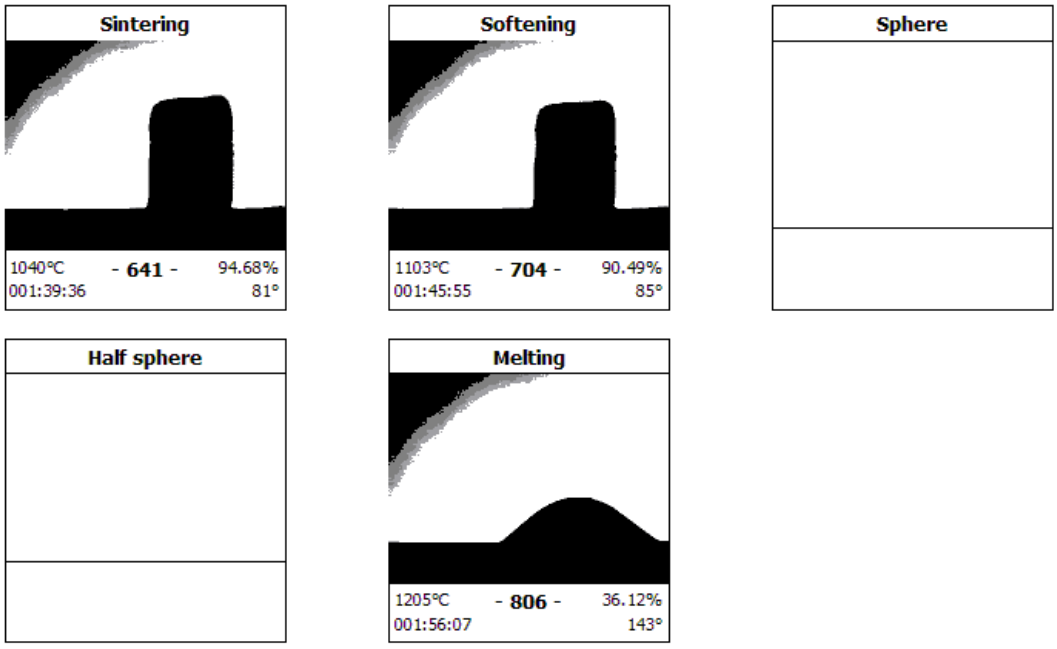

Figure 5. 63-75 µm heated at 10°C/min.

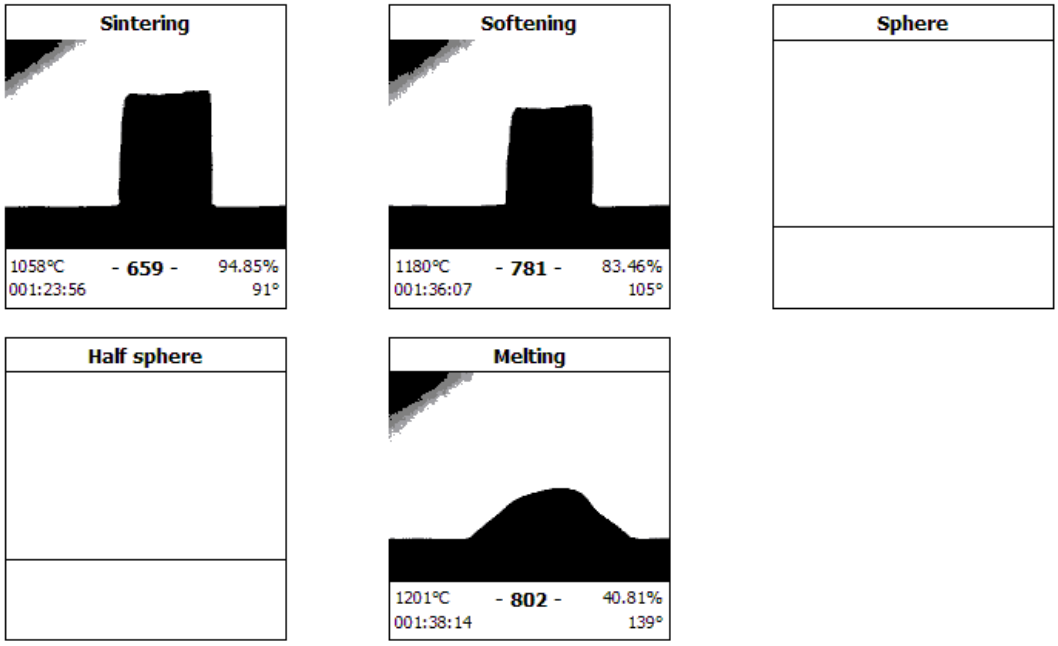

Figure 6. 75-90 µm heated at 10°C/min.

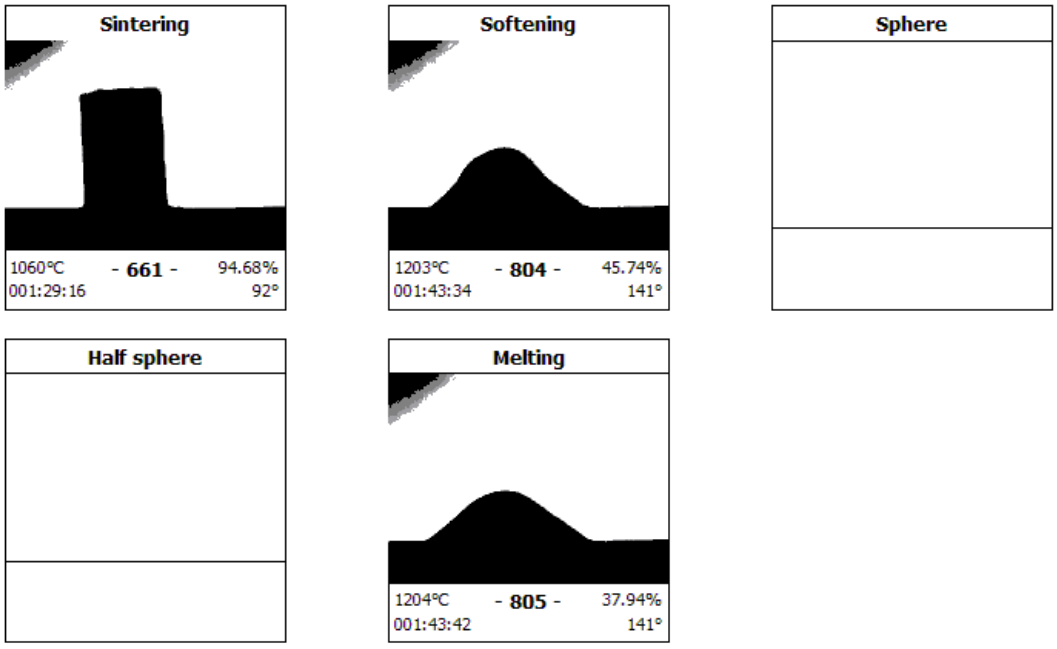

Figure 7. 90-106 µm heated at 10°C/min.

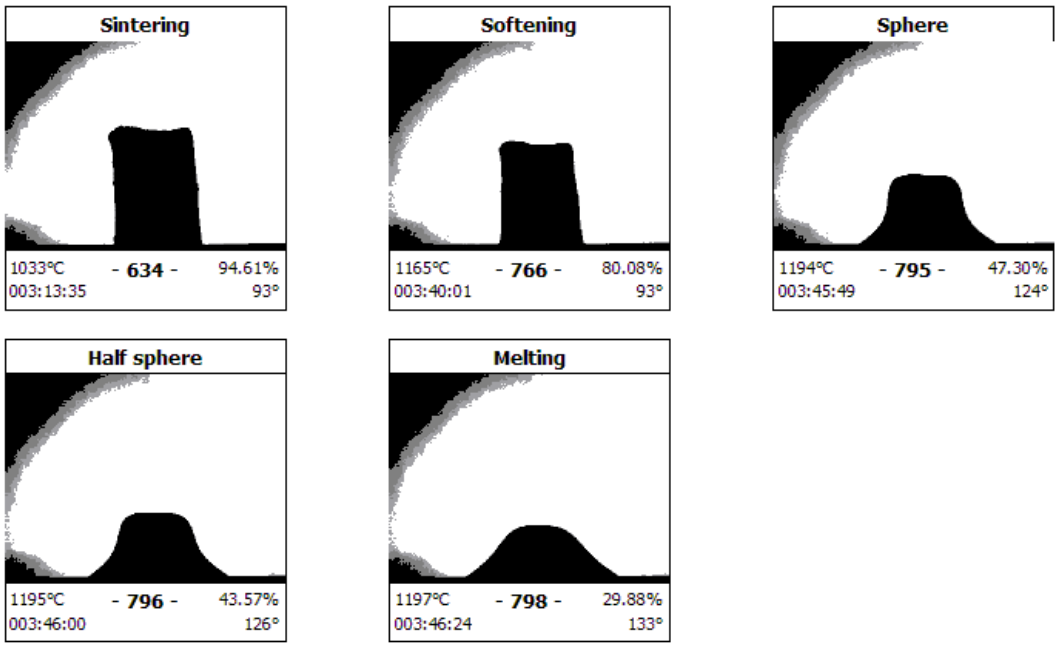

Figure 8. 32-38 µm heated at 5°C/min.

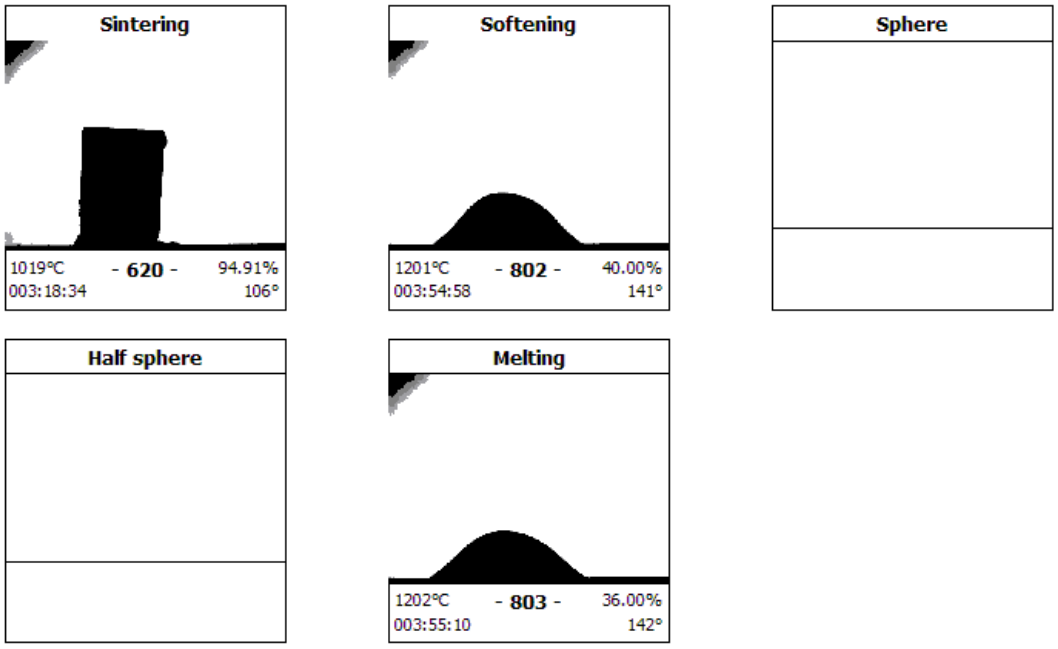

Figure 9. 38-45 µm heated at 5°C/min.

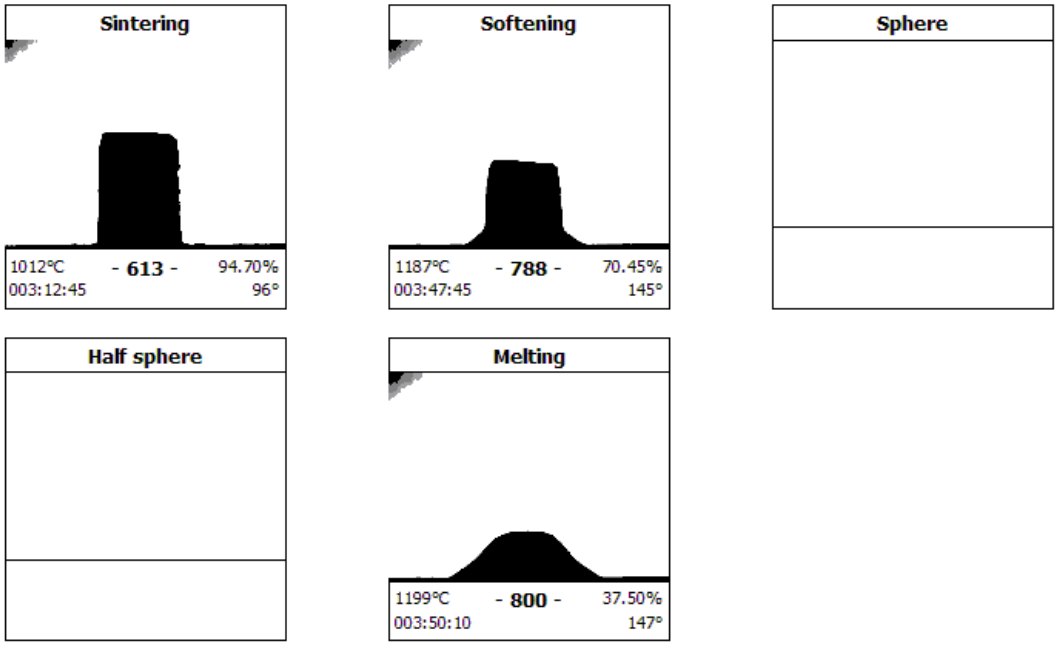

Figure 10. 45-53 µm heated at 5°C/min.

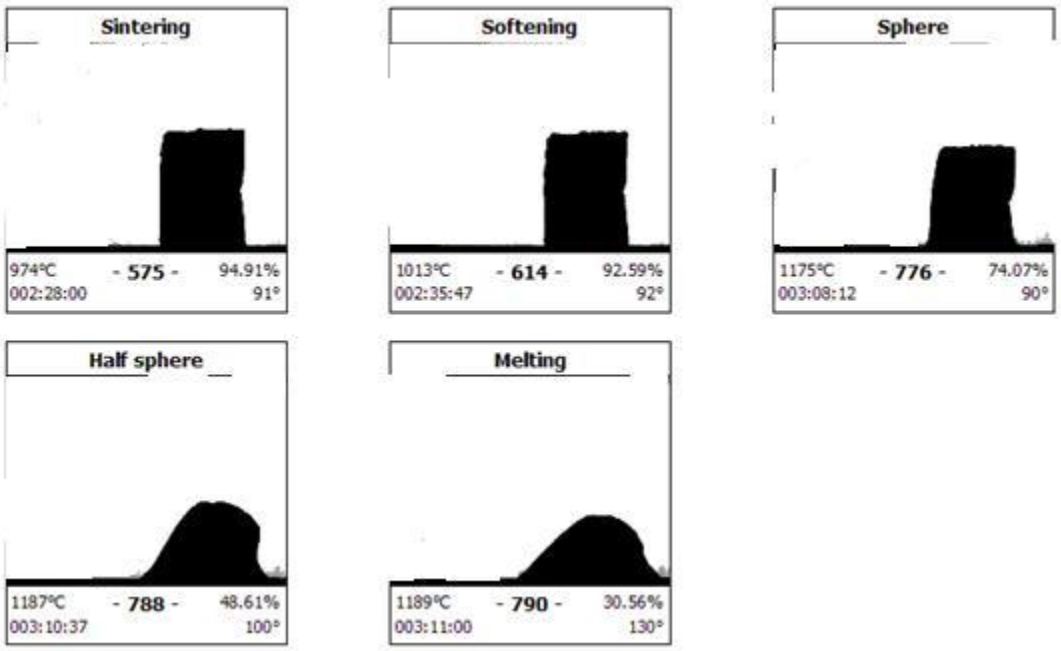

Figure 11. 53-63 µm heated at 5°C/min.

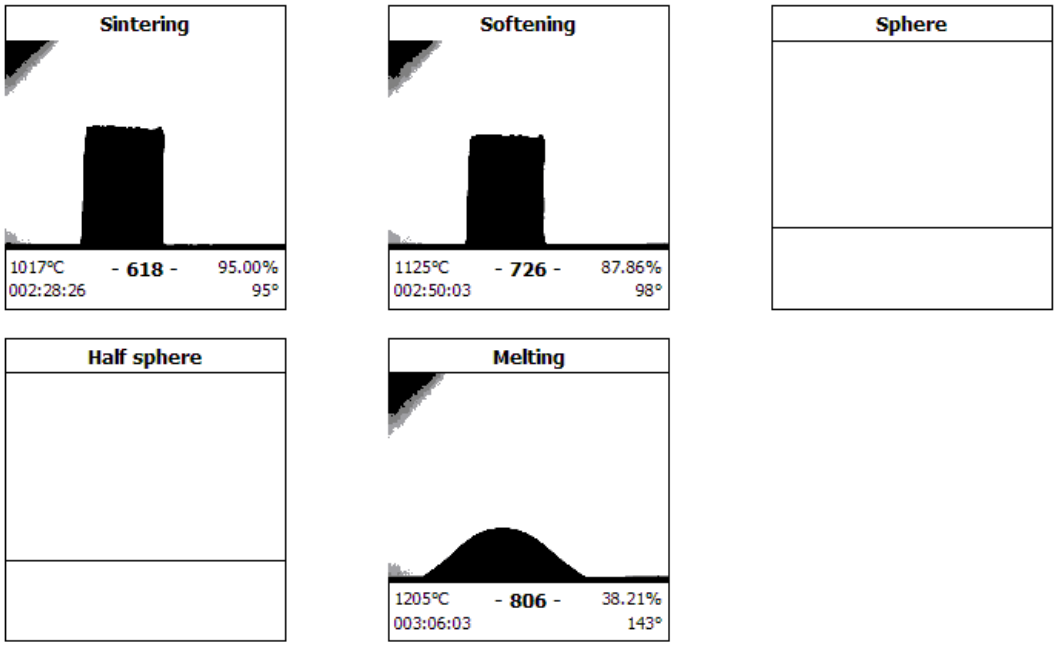

Figure 12. 63-75 µm heated at 5°C/min.

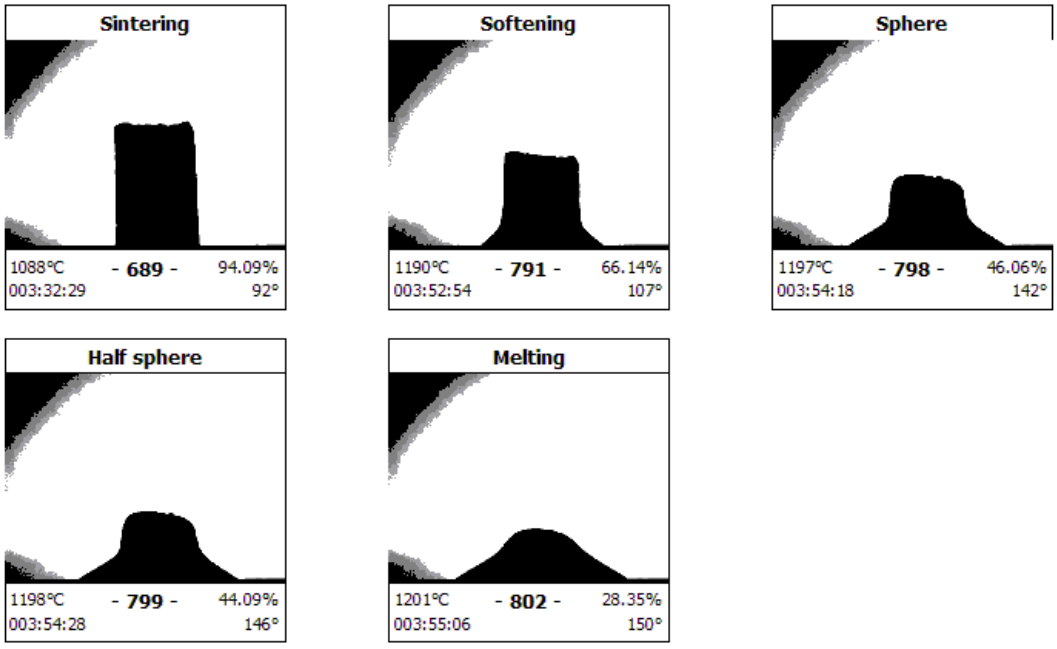

Figure 13. 75-90 µm heated at 5°C/min.

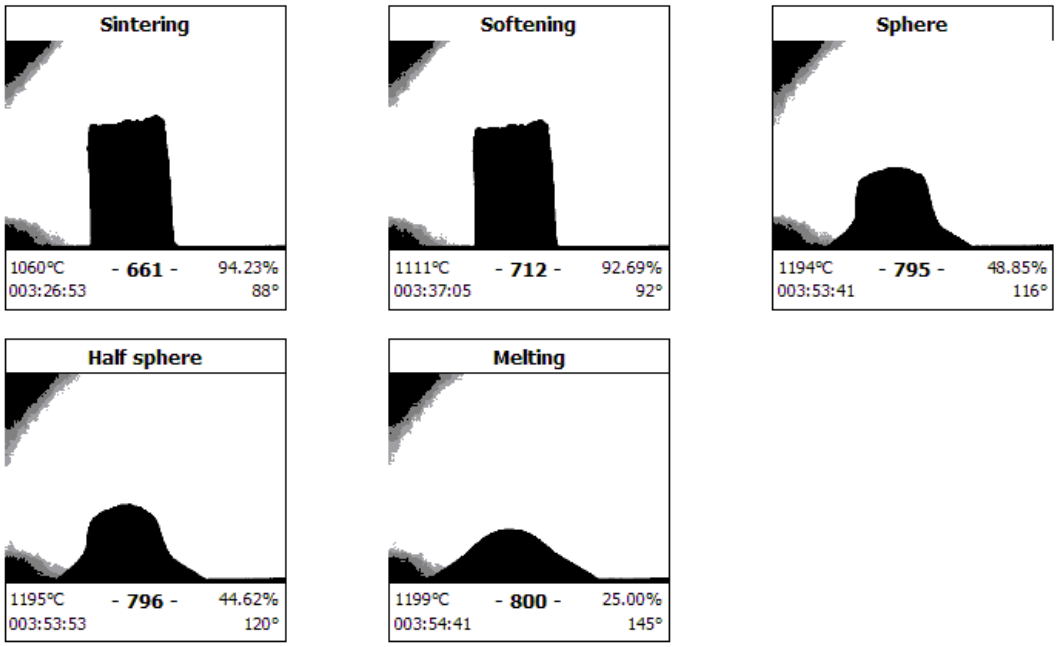

Figure 14. 90-106 μm heated at 5°C/min.

VIII. Literature References

1. Elgayar I, Aliev AE, Boccaccini AR, Hill RG. Structural Analysis of Bioactive Glasses. *J Non-Cryst Solids*. 2005;351(2):173-183.

2. Rahaman MN, Day DE, Bal BS, Fu Q, Jung SB, Bonewald LF, Tomsia AP. Bioactive Glass in Tissue Engineering. *Acta Biomat*. 2011;7(6):2355-2373.

3. Jones JR, Clare AG. *Bio-Glasses: An Introduction*. John Wiley & Sons, Ltd.; 2012.

4. Jones JR, Ehrenfried LM, Hench LL. Optimising Bioactive Glass Scaffolds for Bone Tissue Engineering. *Biomat*. 2006;27(7):964-973.

5. Hoppe A, Guldal N, Boccaccini AR. A Review of the Biological Response to Ionic Dissolution Products from Bioactive Glasses and Glass-Ceramics. *Biomater*. 2011;32:2757-2774.

6. Hench LL. The Story of Bioglass®. *J Mater Sci-Mater M*. 2006;17:967-978.

7. Hu S, Chang J, Liu M, Ning C. Study on Antibacterial Effect of 45S5 Bioglass®. *J Mater Sci-Mater M*. 2009;20:281-286.

8. Julyan AM. Sensodyne to Repair Teeth with Novamin Sealant Technology. Grocer. 234.7995 (Mar. 5, 2011)

9. Deb S, Mandegaran R, Di Silvio L. A Porous Scaffold for Bone Tissue Engineering/45S5 Bioglass® Derived Porous Scaffolds for Co-culturing Osteoblasts and Endothelial Cells. *J Mater Sci-Mater M*. 2010;21(3):893-905.

10. Chen QZ, Thompson ID, Boccaccini AR. 45S5 Bioglass®-derived Glass–ceramic Scaffolds for Bone Tissue Engineering. *Biomat*. 2006;27(11):2414-2425.

11. Bretcanu O,Chatzistavrou X, Paraskevopoulos K, Conradt R, Thompson I, Boccaccini AR. Sintering and Crystallisation of 45S5 Bioglass® Powder. *J Eur Cer Soc*. 2009;29(16):3299-3306.

12. Ch'ng HN, Pan J. Sintering of Particles of Different Sizes. *Acta Mater*. 2007;55"813-824.

13. Robertson IM, Schaffer GB. Some Effects of Particle Size on the Sintering of Titanium and a Master Sintering Curve Model. *Metall Mater Trans A.* 2009;40(8):1968-1979.

14. Francis JSC, Cologna M, Raj R. Particle Size Effects in Flash Sintering. *J Eur Cer Soc*. 2012;32(12):3129-3136.

15. Massera J, Fagerlund S, Hupa L, Hupa M. Crystallization Mechanism of the Bioactive Glasses, 45S5 and S53P4. *J Am Cer Soc*. 2012;95(2):607-613.

16. Arstila H, Vedel E, Hupa L, Hupa M. Factors Affecting Crystallization of Bioactive Glasses. *J Eur Cer Soc*. 2007;27(2–3):1543-1546.

17. Muller R, Zanotto ED, Fokin VM. Surface Crystallization of Silicate Glasses: Nucleation Sites and Kinetics. *J Non-Cryst Solids*. 2000;274:208-231.

18. Lefebvre L, Gremillard L, Chevalier J, Zenati R, Bernache-Assolant D. Sintering Behaviour of 45S5 Bioactive Glass. *Acta Biomat*. 2008;4(6):1894-1903.

19. High Temperature X-ray Diffraction. Rigaku website. 2013. Available at http://www.rigaku.com/applications/high_temp_xray_diffraction. Accessed May 3, 2013.